Title

Structural analysis of mevalonate-3-kinase provides insight into the mechanisms of isoprenoid pathway decarboxylases

Journal

Protein Science, 24(2)

ISSN

0961-8368

Authors

Vinokur, Jeffrey M
Korman, Tyler P
Sawaya, Michael R
et al.

Publication Date

2015-02-01

DOI

10.1002/pro.2607

Peer reviewed

THE PROTEIN SOCIETY

Structural analysis of mevalonate-3-kinase provides insight into the mechanisms of isoprenoid pathway decarboxylases

Jeffrey M. Vinokur, Tyler P. Korman, Michael R. Sawaya, Michael Collazo, Duillio Cascio, and James U. Bowie*

Department of Chemistry and Biochemistry, UCLA-DOE Institute for Genomics and Proteomics, Molecular Biology Institute, University of California, Los Angeles, California 90095-1570

Received 23 October 2014; Accepted 19 November 2014
DOI: 10.1002/pro.2607
Published online 25 November 2014 proteinscience.org

Abstract: In animals, cholesterol is made from 5-carbon building blocks produced by the mevalonate pathway. Drugs that inhibit the mevalonate pathway such as atorvastatin (lipitor) have led to successful treatments for high cholesterol in humans. Another potential target for the inhibition of cholesterol synthesis is mevalonate diphosphate decarboxylase (MDD), which catalyzes the phosphorylation of (R)-mevalonate diphosphate, followed by decarboxylation to yield isopentenyl pyrophosphate. We recently discovered an MDD homolog, mevalonate-3-kinase (M3K) from *Thermoplasma acidophilum*, which catalyzes the identical phosphorylation of (R)-mevalonate, but without concomitant decarboxylation. Thus, M3K catalyzes half the reaction of the decarboxylase, allowing us to separate features of the active site that are required for decarboxylation from features required for phosphorylation. Here we determine the crystal structure of M3K in the *apo* form, and with bound substrates, and compare it to MDD structures. Structural and mutagenic analysis reveals modifications that allow M3K to bind mevalonate rather than mevalonate diphosphate. Comparison to homologous MDD structures show that both enzymes employ analogous Arg or Lys residues to catalyze phosphate transfer. However, an invariant active site Asp/Lys pair of MDD previously thought to play a role in phosphorylation is missing in M3K with no functional replacement. Thus, we suggest that the invariant Asp/Lys pair in MDD may be critical for decarboxylation rather than phosphorylation.

Keywords: mevalonate diphosphate decarboxylase; mevalonate pyrophosphate decarboxylase; mevalonate pathway; mevalonate-3-kinase; mevalonate kinase; GHMP kinase; statin; cholesterol

Introduction

Cholesterol, chlorophyll, and vitamin A are just three examples of over 25,000 biomolecules that make up a diverse class of chemicals called isoprenoids.[1,2] In eukaryotes and some bacteria, isoprenoids are synthesized via the mevalonate pathway, which yields the universal isoprenoid precursor isopentenyl pyrophosphate (IPP).[3] Enzymes of the mevalonate pathway have been heavily investigated for the development of cholesterol lowering drugs.[4–7] Indeed one of the best-selling drugs of all time, atorvastatin (Lipitor), works by inhibiting HMG-CoA reductase, thereby lowering the production of mevalonate.[8] Inhibitors of other mevalonate pathway enzymes such as mevalonate diphosphate decarboxylase

Abbreviations: IPP, isopentenyl pyrophosphate; MDD, mevalonate diphosphate decarboxylase; MVAPP, mevalonate 5-diphosphate; M3K, mevalonate-3-kinase; PDB, protein data bank; RMSD, root-mean-square deviation; 3P-MVAPP, 3-phospho-mevalonate 5-diphosphate.

Additional Supporting Information may be found in the online version of this article.

Grant sponsor: DOE; Grant numbers: DE-FC02-02ER63421, DE-AC02-06CH11357; Grant sponsor: NSF Graduate Research Fellowship; Grant number: DGE-1144087; Grant sponsor: NIH CBI Training Program; Grant number: NIGMS 5T32GM008496; Grant sponsor: NCRR; Grant number: 5P41RR015301-10; Grant sponsor: NIH; Grant number: P41 GM103403.

*Correspondence to: James U. Bowie, No. 659 Boyer Hall, University of California, Los Angeles, 611 Charles E. Young Dr. East, Los Angeles, CA 90095-1570. E-mail: bowie@mbi.ucla.edu

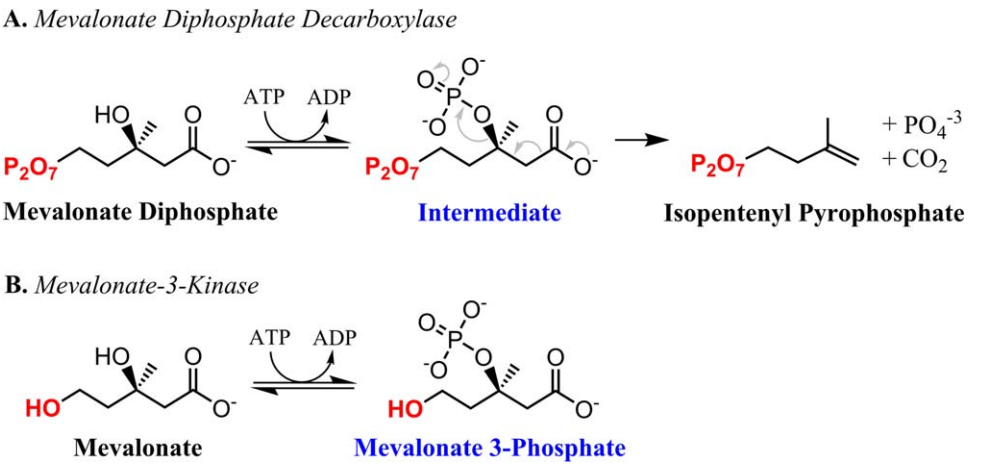

Figure 1. Enzymatic reactions. (A) ATP-dependent phosphorylation catalyzed by mevalonate-3-kinase. (B) Identical phosphorylation catalyzed by mevalonate diphosphate decarboxylase, but with concomitant decarboxylation to yield isopentenyl pyrophosphate.

(MDD) could be useful for lowering cholesterol[9–11] and may also be useful as antimicrobial agents since many pathogens require the mevalonate pathway.[12–14]

MDD converts (R)-mevalonate 5-diphosphate (MVAPP) and ATP to isopentenyl pyrophosphate (IPP), ADP, PO_4, and CO_2.[15] As shown in Figure 1(A), the mechanism can be conceptually divided into two stages, phosphorylation and decarboxylation. The phosphorylation stage involves transfer of the γ-phosphate of ATP to the 3-OH position of MVAPP, generating the intermediate, 3-phosphomevalonate 5-diphosphate (3P-MVAPP) [Fig. 1(A)].[16–18] This intermediate was originally thought to spontaneously decompose to IPP, CO_2 and PO_4 due to the instability of the sterically hindered tertiary phosphate,[14,19] but we recently reported the analogous tertiary phosphorylated intermediates, mevalonate 3-phosphate and mevalonate 3,5-bisphosphate are both stable.[20] Moreover, a fluorinated version of 3P-MVAPP was reported to be stable after isolation from a quenched MDD reaction.[21] It is therefore likely that decarboxylation is not spontaneous so that MDD must also catalyze the decarboxylation step.

We were recently presented with a unique opportunity to probe the mechanism of MDD, by our discovery, along with another group, of a novel mevalonate pathway enzyme, mevalonate-3-kinase (M3K,) in the archeon *Thermoplasma acidophilum*.[20,22] M3K catalyzes the ATP dependent phosphorylation of (R)-mevalonate to produce (R)-mevalonate 3-phosphate, but without concomitant decarboxylation [Fig. 1(B)].[20] Instead, mevalonate 3-phosphate is released as a stable metabolite. A second enzyme phosphorylates the 5-OH position to yield mevalonate 3,5-bisphosphate, which has been proposed to ultimately be decarboxylated and phosphorylated to the universal isoprenoid building block IPP, although the decarboxylase has not yet been identified.[20,22] While M3K does not decarboxylate, it does phosphorylate mevalonate in the same position as the homologous decarboxylases, and shares 17–21% sequence identity with MDDs from *H. sapiens*, *S. epidermidis*, and *S. cerevisiae*. Thus, M3K can be considered a defective decarboxylase that catalyzes exactly half the overall reaction of MDD.

To provide insight into the mechanism of MDD, we solved the crystal structure of M3K in the *apo* form and with bound substrates and product, allowing us to perform structural comparisons to MDD, for which nineteen structures have been reported (*H. sapiens, M. musculus, T. brucei, S. cerevisiae, L. pneumophila, S.aureus, S. pyogenes, S. epidermidis*).[14,19,23–25] Analysis of the M3K active site identified two residues involved in catalyzing phosphate transfer, Arg185 and Ser105, and also identified how M3K binds mevalonate, while excluding mevalonate 5-phosphate and mevalonate 5-diphosphate. Comparison to MDD leads us to propose a model in which both enzymes use similar residues (Arg185/Ser105 in M3K and Lys188 in MDD) to catalyze phosphorylation and we suggest that the invariant Asp/Lys pair unique to MDD plays a critical role in the decarboxylation step rather than phosphorylation.

Results and Discussion

Overall fold

M3K crystalized in space group C2 with two protein molecules in the asymmetric unit [Fig. 2(A)] that are linked by a disulfide bond between Cys 43 from each monomer. The enzyme purified primarily as a

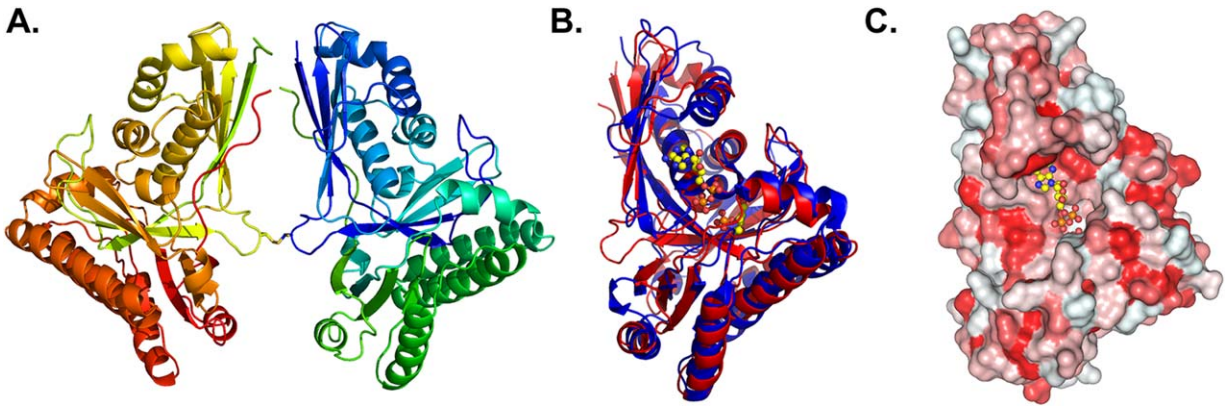

Figure 2. Overall structure of M3K. (A) The asymmetric unit of M3K highlighting the disulfide bond between the two proteins. (B) Overlay of M3K (red) with *S. epidermidis* MDD (blue) shows a nearly identical overall fold. (C) M3K surface rendering using a hydrophobicity scale[26] shows the deep active site cleft. Red indicates hydrophobic residues and white indicates hydrophilic residues.

dimer, and became monomeric in the presence of 1 m*M* β-mercaptoethanol (Supporting Information Fig. S1). The monomeric and dimeric forms had equal activity under optimal conditions (pH 8.5 and 55°C). Some archaea are known to possess disulfide bonded proteins in the cytoplasm,[27–29] and the M3K dimer is slightly more stable (Supporting Information Fig. S2), suggesting that the natural form of the protein could be a dimer.

We compared our M3K structures to the structure of MDD from *S. epidermidis* (PDB: 4DU7), since the *S. epidermidis* structure contained a bound mevalonate diphosphate (MVAPP), marking the active site.[25] When the M3K *apo* structure is overlayed with the MDD structure from *S. epidermidis*, they align with an overall backbone RMSD of 2.40 Å, despite sharing only 19% sequence identity [Fig. 2(B)]. For comparison, the backbone atoms of *S. epidermidis* MDD compared to those of the MDD enzyme from *S. cerevisiae* have an overall RMSD of 2.15 Å. The high structural similarity places M3K into the GHMP kinase family (Galactokinase, Homoserine kinase, Mevalonate kinase, and Phosphomevalonate kinase).[30] All members of this family share a highly conserved overall fold that contains a centrally located cleft with the active site located at the base of the cleft [Fig. 2(C)].[31]

The mevalonate binding pocket

To obtain insight into substrate binding and catalysis, we determined a structure of M3K bound to (R)-mevalonate, and a structure of M3K bound to both (R)-mevalonate 3-phosphate and ADP. Mevalonate was found in both proteins of the asymmetric unit [Fig. 3(A)]; however, mevalonate 3-phosphate and ADP were only observed in chain A [Fig. 3(B)]. Chain B contained mevalonate 3-phosphate in the same position as in chain A, but the ADP was replaced with a density modeled as a sulfate ion.

The structures revealed no major conformational shifts when binding to substrate or products. Global backbone RMSD for all pairwise comparisons of the M3K structures (six molecules) did not exceed 0.38 Å. The pair with the largest deviation was chain A of the substrate complex and chain B of the

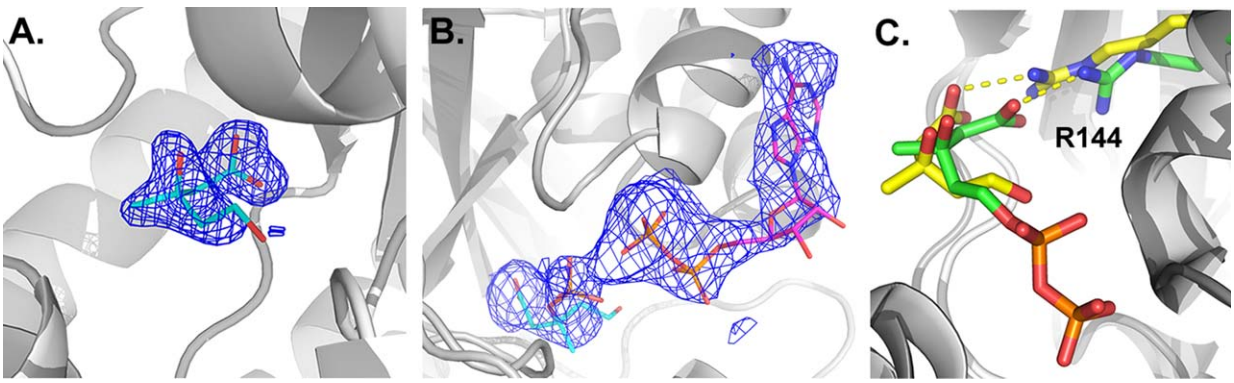

Figure 3. Substrate binding to M3K. (A) Electron density for mevalonate. The blue mesh is a simulated annealing F_o-F_c omit map contoured at 2.5 σ. The omit map was obtained by subjecting the refined protein coordinates without ligands to a round of simulated annealing refinement starting at 10,000 K. (B) A simulated annealing F_o-F_c omit map for mevalonate 3-phosphate and ADP, generated in same manner as mevalonate and contoured at 1.9 σ. (C) M3K with bound mevalonate (yellow) is overlayed against MDD with bound mevalonate diphosphate (green) showing the conserved binding location.

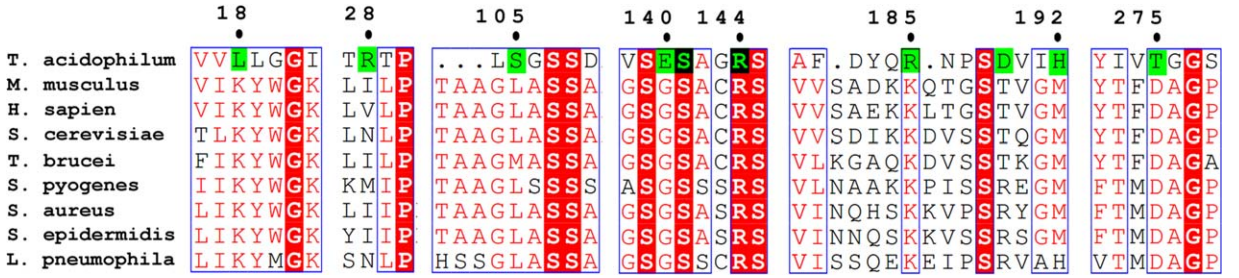

Figure 4. Sequence alignment of M3K and MDDs. A structure-based amino acid sequence alignment of M3K from *T. acidophilum* (Ta1305) aligned against the sequences of eight known MDD structures. The numbering corresponds to M3K and residues discussed in this paper are highlighted in green.

product complex. When we restricted analysis to the active site of this pair (residues within 5 Å of bound mevalonate 3-phosphate), we found an RMSD of only 0.31 Å (116 atoms). This high degree of structural conservation is also seen in the active site cores of all known MDD structures.[14] These results suggest that M3K does not require major conformational shifts for catalysis.

Mevalonate and mevalonate 3-phosphate bind in the center of a deep cleft located in the middle of the enzyme [Fig. 2(C)]. This is the same location that MVAPP binds in MDD.[25] The orientation of mevalonate in M3K is rotated by 31° relative to MVAPP [Fig. 3(C)]. This is due to a 1.8 Å shift in the positioning of Arg144 (Fig. 4), which binds the carboxylate moiety of mevalonate in both enzymes. Mevalonate is not translated with respect to MVAPP, however, as the C3 carbons of both species are only 0.7 Å apart.

MDD binds the pyrophosphate moiety of MVAPP primarily through four invariant serine residues[25] [Fig. 5(A)]. In M3K, the pyrophosphate does not fit due to the protrusion of Glu140 into the middle of the active site. Glu140 replaces an invariant glycine at the analogous position in MDD (Fig. 4) and provides a polar contact directly to the 5-OH tail of mevalonate. Mevalonate's position in the center of the active site cavity is stabilized by a web of polar contacts made by His192, Arg28, and Asp189 [Fig. 5(B)]. Additionally, an invariant serine (Ser141) in both M3K and MDD can provide an additional hydrogen bond to the 5-OH tail of mevalonate. The steric hindrance introduced by Glu140 explains why mevalonate 5-phosphate and mevalonate 5-diphosphate are not phosphorylated by M3K.[20]

Residues important for phosphate transfer

Both Arg185 and Ser105 in M3K make polar contacts to the transferred phosphate and the β-phosphate of ADP [Fig. 6(A)]. Arg185 is oriented towards the broken P-O bond, 3.4 Å from the β-phosphate of ADP and 3.3 Å from the transferred

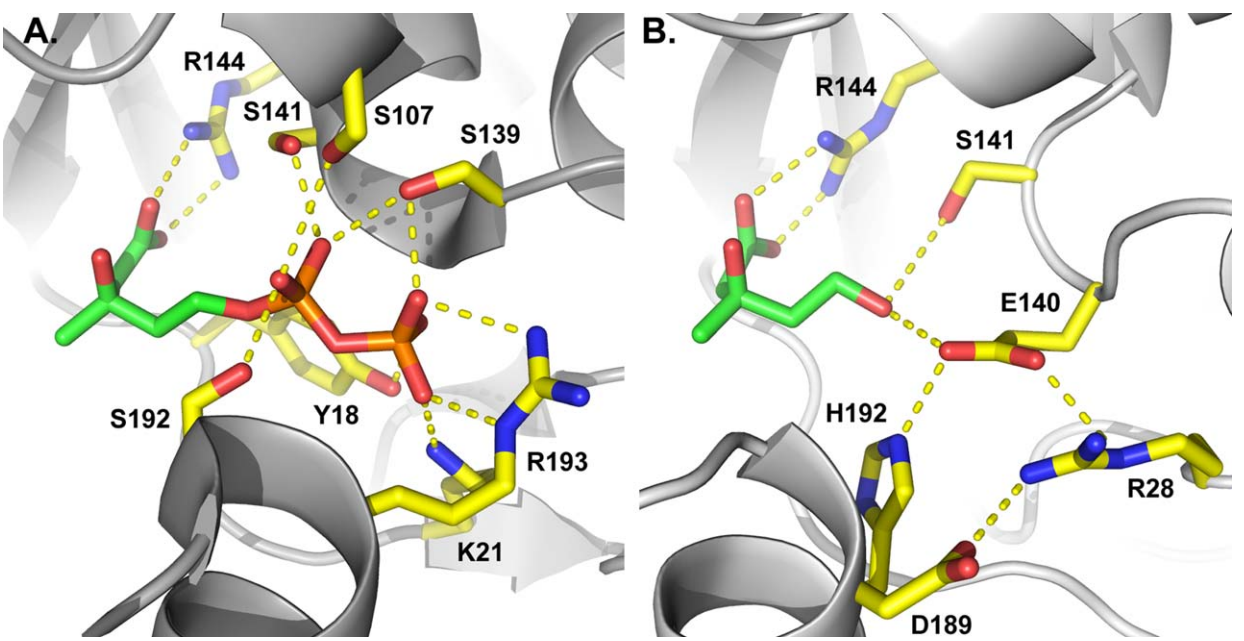

Figure 5. Binding site comparison of MDD and M3K. (A) *S. epidermidis* MDD active site highlighting residues that make polar contacts to the pyrophosphate. (B) M3K active site showing Glu140 and the web of polar contracts that engage the 5-OH tail of mevalonate.

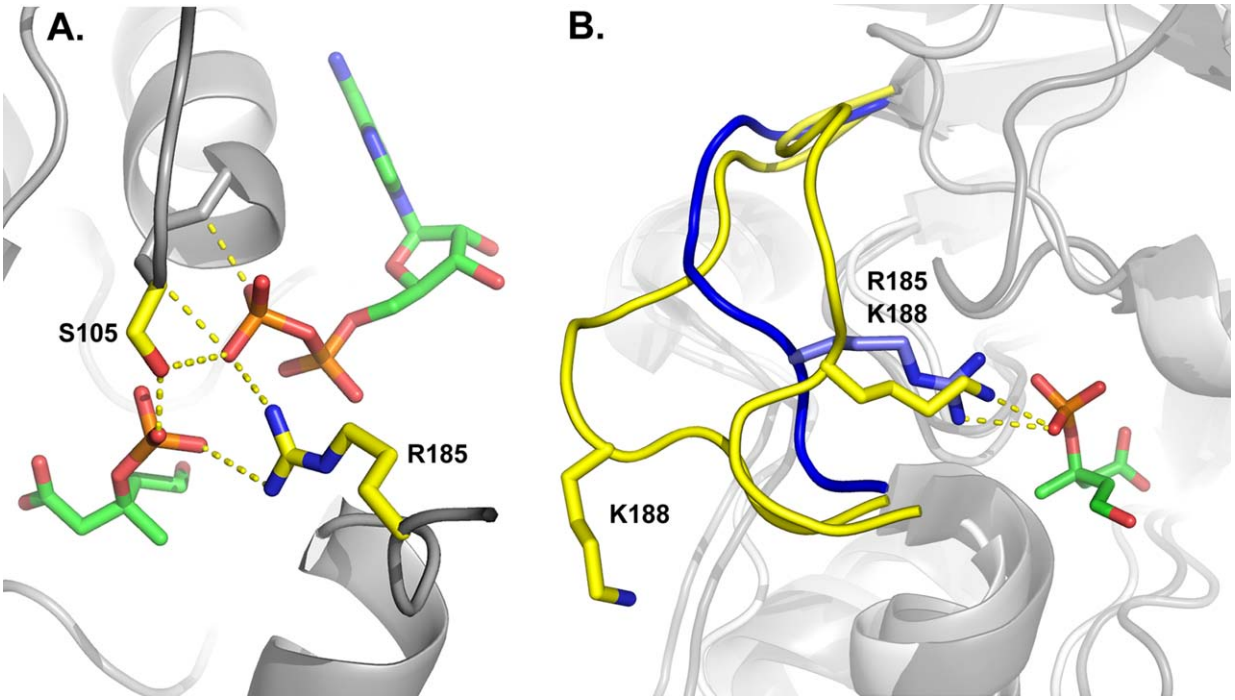

Figure 6. Catalysis of phosphate transfer. (A) Polar contacts of Arg185 and Ser105 to mevalonate 3-phosphate and ADP. (B) The two conformations of the flexible loop of MDD. The outward conformation (yellow) is from *L. pneumophila*, and the inward conformation (also yellow) is a D283A mutant from *S. epidermidis*. Lys188 of MDD (yellow) overlays with Arg185 of M3K (blue) when the loop is oriented inward.

phosphate, which is close enough to provide important stabilizing interactions in the transition state.

Arg185 of M3K aligns with an invariant lysine (Lys188) in MDD (Fig. 4), both of which are located in a loop region. Surprisingly, this loop is disordered in all wild type MDD structures from *S. epidermidis*; however, a D283A mutant of *S. epidermidis*[25] captured this flexible loop in a secondary conformation, where Lys188 of MDD spatially overlays with Arg185 from M3K [Fig. 6(B)]. Lys188 is important for catalysis as a K188A mutant in MDD abolishes all activity.[32] We prepared a R185A mutant in M3K, which also resulted in no detectable activity. To demonstrate an analogous relationship between R185 of M3K and K188 of MDD, we prepared a R185K mutant of M3K, which was active (Table I). Thus, it is likely that the invariant Lys188 in MDD plays a similar role to Arg185 in M3K, directly stabilizing a phospho-transfer transition state.

Ser105 of M3K is also oriented towards the broken P-O bond. Ser105 is located in a loop region and spatially aligns between conserved Leu and Ala residues in MDD (Fig. 4). Ser105 is 2.4 Å from the transferred phosphate and 3.4 Å from the β phosphate of ADP. An S105A mutant resulted in a 4.6 fold decrease in k_{cat}, with only a marginal increase in K_m (Table I), consistent with a modest role in stabilizing the transition state in phosphate transfer. The transition state is likely further stabilized by hydrogen bonds between the phosphates and amide groups from the protein backbone [Fig. 6(A)].

Table I. *Kinetic Parameters of M3K Variants*

Mutation	K_m (μM)[a]	k_{cat} (s^{-1})[a]	$k_{cat}/K_m \times 10^3$ (%)[b]
Wildtype	130 ± 10	5.3 ± 0.1	39 ± 9 (100%)
T275A	590 ± 40	5.8 ± 0.1	10 ± 3 (25.6%)
L18A	3100 ± 200	5.1 ± 0.1	1.7 ± 0.5 (4.4%)
S105A	270 ± 10	1.16 ± 0.01	4 ± 1 (10.3%)
R185K	1680 ± 60	0.31 ± 0.01	0.19 ± 0.05 (0.5%)
R185A	0.0[c]	0.0[c]	—

[a] In the presence of 5 mM ATP, which was found to be sufficient to saturate all the enzyme variants. The Michaelis-Menten plots are shown in the Supporting Information.
[b] Percentage values of k_{cat}/K_m are relative to wildtype M3K.
[c] Rate not detectable. The minimum detectable rate of the coupled assay is 0.2% relative to wildtype activity.

Residues involved in decarboxylation

All MDDs have three invariant residues within the active site (Arg144, Asp283, and Lys17 in *S. epidermidis* MDD).[25] Arg144 positions the substrate in the active site [Fig. 3(C)], and the Asp283/Lys17 pair has been proposed to directly deprotonate the 3-OH of MVAPP, triggering phosphorylation.[15–17] The catalytic role for the invariant Asp/Lys pair of MDD is supported by its active site position and previous mechanistic studies, which showed that a D283A mutant yields a 10^5 fold reduction in activity,[33] and a K17A mutant yields no detectable activity.[32]

In M3K, Arg144 is conserved for positioning the mevalonate moiety, but the invariant Asp/Lys pair

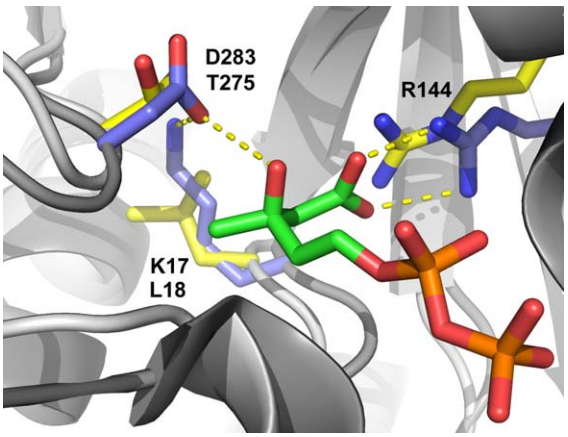

Figure 7. Resides implicated in decarboxylation. The invariant MDD residues of *S. epidermidis* are show in blue (Arg144, Lys17, and Asp283). In M3K, Lys17 of MDD is replaced by Leu18 (yellow) and Asp283 is replaced by Thr275 (also yellow).

in MDD is replaced by Leu18 and Thr275 in M3K, respectively (Fig. 7). To test the role of Leu18 and Thr275, we characterized mutants L18A and T275A. Both L18A and T275A mutants had no significant effect on k_{cat} while slightly increasing K_m. Thus, these residues are not involved in kinase activity (Table I).

Some members of the GHMP kinase family, such as homoserine kinase (PDB: 1H72) are known to facilitate phosphate transfer without the presence of an active site Asp/Lys pair,[34] yet others such as mevalonate 5-kinase (PDB: 2HUF) and phosphomevalonate kinase (PDB: 3GON) have an active site Asp/Lys pair.[35,36] These observations have led to two proposed mechanisms of phosphate transfer, one involving simple transition state stabilization, and a second involving Asp/Lys mediated deprotonation, followed by nucleophilic attack on the γ-phosphate of ATP.[14] The current data raises a third possibility.

We propose M3K and MDD both phosphorylate by stabilizing the phospho-transfer transition state (M3K via Arg185/Ser105, MDD via Lys188), leaving the invariant Asp/Lys pair, unique to MDD, to play a role in the decarboxylation step. Testing this model has proven difficult since mutating D283 in MDD to Ala, Glu, Thr, Val or Asn results in no detectable kinase activity. This was explained by a crystal structure of a D283A mutant from Barta *et al*.,[25] in which the mutation caused catastrophic changes in MVAPP binding orientation. Barta *et al*. suggest D283 may play a critical role in positioning the substrate. We can rule out the pyrophosphate moiety as the differentiating factor needed for decarboxylation as a recently characterized enzyme, mevalonate monophosphate decarboxylase from *Haloferax volcanii*[37] and *Roseiflexus castenholzii*[38] were shown to catalyze the identical reaction as MDD, but with mevalonate 5-phosphate. A PHYRE (Protein Homology/Analogy Recognition Engine)[39] model of both mevalonate monophosphate decarboxylases showed retention of the Asp/Lys pair in the same position as MDD, consistent with a role in decarboxylation (Supporting Information Fig. S8).

Conclusions

The crystal structure of mevalonate-3-kinase provides new insight into the mechanism of mevalonate diphosphate decarboxylase. Despite sharing nearly identical overall folds, important active site differences can be identified. Glu140 in the center of the M3K active site is responsible for binding mevalonate while excluding mevalonate 5-diphosphate, Arg185/Ser105 catalyze phosphate transfer, and an invariant Asp/Lys pair previously thought to be responsible for phosphorylation in MDD, is missing in M3K and replaced by non-essential Thr275/Leu18. These findings lead us to propose a model in which M3K and MDD both phosphorylate by stabilizing a phospho-transfer transition state (M3K via Arg185/Ser105, MDD via Lys188), suggesting the invariant Asp/Lys pair unique to MDD may be critical for the decarboxylation step rather than phosphorylation.

Methods

M3K expression, purification and assays

M3K expression, purification and enzyme assays were all conducted as reported previously.[20] In summary, the *ta1305* gene (encoding mevalonate-3-kinase) was cloned into a pET28 plasmid, providing an N-terminal His tag. The plasmid was transformed into *E. coli* BL21 Gold (DE3), cells were grown in LB-media supplemented with 50 mg/L kanamycin, and protein production was induced with 0.5 m*M* IPTG for 20 h at 37°C. M3K was purified by Ni-NTA affinity chromatography followed by elution with 250 m*M* imidazole. Further purification was accomplished by gel filtration on a Superdex S200 column in 50 m*M* Tris-HCl pH 7.5 and 100 m*M* NaCl.

Crystal growth conditions

A stock of M3K was prepared by concentrating the protein in 7 m*M* Tris-HCl pH 7.5 and 45 m*M* NaCl to 7.0 mg/mL using a 30 kDa cutoff Amicon Ultra-15 centrifugal filter (Millipore) and stored at 4°C. Some precipitation of the stock was observed upon cooling, but it clarified upon incubation at room temperature for 5 min. Crystallization conditions were screened using the hanging drop method[40] in 96 well plates. For each condition, three 210 nL hanging drops with varying protein stock to reservoir ratios (2:1, 1:1, 1:2) were prepared using a TTP LabTech Mosquito nanoliter-pipetting robot in the UCLA Macromolecular Crystallization Facility. Large single crystals grew after 2 days in ProComplex condition 68, (Quiagen Cat No. 135468A) which consists of 0.1 *M* sodium acetate pH 5.0 and 1.0 *M* ammonium sulfate (2:1 protein:reservoir

ratio). Crystals were cryo-protected by a quick soak in a solution consisting of 65% reservoir, 35% (v/v) glycerol, then flash frozen in a cryogenic nitrogen stream and maintained at 100 K for data collection.

Binding of substrate and products

Substrate complex crystals were obtained by soaking substrates into the *apo* crystals that were prepared as described above. For the mevalonate soaks, a single crystal was removed from the hanging drop and placed directly into 8 μL of 65 m*M* (R)-mevalonate for 2 h (no mother liquor). During the soak, the crystal morphology remained intact without cracking or dissolving. The crystal was removed from the mevalonate solution and quickly cryo-protected with 20% glycerol, 80% 65 m*M* (R)-mevalonate solution, and placed into a cryogenic nitrogen stream for data collection. To bind products, a mixture of 25 m*M* (R)-mevalonate 3-phosphate and 25 m*M* ADP was prepared enzymatically in a 1 mL reaction consisting of 25 m*M* (R)-mevalonate, 25 m*M* ATP, 1 m*M* $MgCl_2$, and 36 μg mevalonate-3-kinase. The reaction was incubated at 42°C for 1 h, then cooled to room temperature before attempting crystal soaks. About 2 μL of the product solution was mixed with 8 μL of mother liquor so the final concentration of products was approximately 5 m*M*. A crystal soaked in this 5 m*M* solution for 40 min was rapidly transferred into a solution of 35% glycerol, 65% mother liquor for 5 s and placed into the cryogenic nitrogen stream for data collection.

X-Ray data collection

X-ray diffraction data for the *apo* (2.1 Å) and substrate (2.0 Å) crystals were collected with a Rigaku FR-E rotating anode X-ray source, using CuKα radiation (λ = 1.5418 Å) and an R-AXIS HTC imaging plate detector. Data for crystals soaked with products were first collected in-house, and then flash frozen and shipped to the Advanced Photon Source (Argonne National Laboratory) for data collection on APS-NECAT beamline 24-ID-C with a DECTRIS-PILATUS 6 *M* detector. A crystal soaked with products diffracted to 2.3 Å on the APS beamline. Reduction and scaling of data were performed using XDS/XSCALE.[41] All data sets were consistent with space group C2 (Supporting Information Table S1).

Structure determination and refinement

The *apo* structure was determined using the automated molecular replacement pipeline, MrBUMP.[42] The path that led to a successful solution employed PHASER[43] for molecular replacement and a search model prepared by CHAINSAW[44] from PDB entry 1FI4, mevalonate 5-diphosphate decarboxylase.[24] Trimming of the 1FI4 coordinate set by CHAINSAW was important for success as the full coordinate set did not lead to a correct molecular replacement solution. The sequence identity between TA1305 and 1FI4 is under 20%. The *apo* model was initially refined using Refmac5[45] with no non-crystallographic symmetry restraints. The residual F_o-F_c map showed clear positive difference density for side chain atoms that were not included in the model, indicating the correctness of the solution. The automatic chain tracing program, Buccaneer,[46] built in missing parts of the model. This was followed by automated building and refinement with the program ARP/wARP.[47] After each refinement step, the models were visually inspected in COOT,[48] and modified using guidance from both $2F_o$-F_c and F_o-F_c difference maps. Structures for substrate and product bound data sets were solved by refinement against the *apo* structures using phenix.refine.[49] Data collection and refinement statistics are reported in Supporting Information Table S1. The models were validated with PROCHECK,[50] ERRAT,[51] and VERIFY3D.[52] The coordinates of the final models and structure factors have been deposited in the Protein Data Bank with PDB code 4RKP (apo), 4RKS (substrate), and 4RKZ (products). The structures were illustrated using Pymol[53] and compared to *S. epidermidis* MDD (PDB: 4DU7 and 4DPW) with MDD residues numbered as per their PDB files.

Mutagenesis

About 100 ng of pET28a plasmid containing the *ta1305* gene was subjected to 32 cycles of the PCR protocol outlined in the manual of PfuUltra II Fusion HS DNA Polymerase (Agilent Cat No. 600670). Mutagenic primers were designed using PrimerX.[54] About 50 μL of the completed PCR reaction was treated with 1 μL DpnI (New England Biolabs) for 1 h at 37°C, and then 3 μL was used to transform 100 μL of *E. coli* BL21 Gold (DE3) cells. Transformants were selected on LB-agar containing 50 μg/mL kanamycin. Mutations were verified by sequencing the plasmid from the T7 promoter.

Kinetic values for M3K variants

Kinetic measurements for all mevalonate-3-kinase variants were carried out in duplicate on a SpectraMax M5 microplate reader. Continuous monitoring of M3K activity under optional conditions (pH 8.5 and 55°C) was achieved through a coupled kinase assay as previously described in detail.[20] Initial rates of ATP consumption were determined over a range of (R)-mevalonate concentration, while holding ATP at a saturating concentration of 5 m*M*. These values were plotted with KaleidaGraph, version 4.0 (Synergy Software, Reading, PA, USA) and fit to a Michaelis-Menten curve to yield K_m and k_{cat} values with respect to (R)-mevalonate.

Sequence alignment

A pdb structure for M3K (*apo*) and 8 known MDD structures from the Protein Data Bank (*H. sapiens,*

M. musculus, T. brucei, S. cerevicie, L. pneumophila, S. aureus, S. epidermidis, S. pyogenes) were submitted to PROMALS3D, a structure alignment server.[55] The output sequences were edited with Macromedia Fireworks MX 2004[56] to improve loop alignment and to fill in structurally disordered residues. The final alignment was rendered with Espript 3.0.[57]

Comparison of monomer and dimer activity

Monomer was prepared by incubating enzyme with 1 m*M* β-mercaptoethanol for 1 h at 37°C, and dimer was prepared by incubating the enzyme with 100 μ*M* copper acetate complexed with 100 μ*M* 1,10-phenanthroline for 1 h at 37°C. Heat stability was tested by incubating 0.16 mg/mL of both enzyme forms at 40–81°C for 60 min in increments of 1–3°C. After heating, residual activity was tested as described previously in an assay buffer without reducing agent.[20]

Acknowledgments

We thank members of the Bowie Lab for critical reading of this manuscript.

References

1. Holstein SA, Hohl RJ (2004) Isoprenoids: remarkable diversity of form and function. Lipids 39:293–309.
2. Goldstein JL, Brown SB (1990) Regulation of the mevalonate pathway. Nature 343:425–430.
3. Katsuki H, Bloch K (1967) Studies on the biosynthesis of ergosterol in yeast. Formation of methylated intermediates. J Biol Chem 242:222–227.
4. Buhaescu I, Izzedine H (2007) Mevalonate pathway: a review of clinical and therapeutical implications. Clin Biochem 40:575–584.
5. Istvan ES (2002) Structural mechanism for statin inhibition of 3-hydroxy-3-methylglutaryl coenzyme A reductase. Am Heart J 144:S27–S32.
6. Qiu Y, Li D (2006) Bifunctional inhibitors of mevalonate kinase and mevalonate 5-diphosphate decarboxylase. Org Lett 8:1013–1016.
7. Brown MS, Goldstein JL (1986) A receptor-mediated pathway for cholesterol homeostasis. Science 232:34–47.
8. Sever PS, Dahlöf B, Poulter NR, Wedel H, Beevers G, Caulfield M, Collins R, Kjeldsen SE, Kristinsson A, McInnes GT, Mehlsen J, Nieminen M, O'Brien E, Östergren J (2003) Prevention of coronary and stroke events with atorvastatin in hypertensive patients who have average or lower-than-average cholesterol concentrations, in the Anglo-Scandinavian Cardiac Outcomes Trial: a multicenter randomized controlled trial. The Lancet 361:1149–1158.
9. Gonzalez-Pacanowska D, Marco C, Garcia-Martinez J, Garcia-Peregrin E (1985) Role of mevalonate-5-pyrophosphate decarboxylase in the regulation of chick intestinal cholesterogenesis. Biochim Biophys Acta 833: 449–455.
10. Qiu Y, Li D (2006) Inhibition of mevalonate 5-diphosphate decarboxylase by fluorinated substrate analogs. Biochim Biophys Acta 1760:1080–1087.
11. Vlattas I, Dellureficio J, Ku E, Bohacek R, Zhang X (1996) Inhibition of mevalonate 5-pyrophosphate decarboxylase by a proline-containing transition state analog. Bioorg Med Chem Lett 6:2091–2096.
12. Heuston S, Begley M, Gahan CGM, Hill C (2012) Isoprenoid biosynthesis in bacterial pathogens. Microbiology 158:1389–1401.
13. Wilding EI, Brown JR, Bryant AP, Chalker, AF, Holmes DJ, Ingraham KA, Iordanescu S, So CY, Rosenberg M, Gwynn MN (2000) Identification, evolution, and essentiality of the mevalonate pathway for isopentenyl diphosphate biosynthesis in gram-positive cocci. J Bacteriol 182:4319–4327.
14. Barta ML, Skaff DA, McWhorter WJ, Herdendorf TJ, Miziorko HM, Geisbrecht BV (2011) Crystal structures of *Staphylococcus epidermidis* mevalonate diphosphate decarboxylase bound to inhibitory analogs reveal new insight into substrate binding and catalysis. J Biol Chem 286:23900–23910.
15. Jabalquinto AM, Alvear M, Emil EC (1988) Minireview: physiological aspects and mechanism of action of mevalonate 5-diphosphate decarboxylase. Comp Biochem Physiol 90:671–677.
16. Lindberg M, Yuan C, de Waard A, Bloch K (1962) On the formation of isopentenyl pyrophosphate. Biochemistry 1:182–188.
17. Iyengar R, Cardemil E, Frey PA (1986). Mevalonate-5 diphosphate decarboxylase: stereochemical course of ATP-dependent phosphorylation of mevalonate 5-diphosphate. Biochemistry 25:4693–4698.
18. Skilleter DN, Kekwick RG (1971) The enzymes forming isopentenyl pyrophosphate from 5-phosphomevalonate (mevalonate 5-phosphate) in the latex of *Hevea brasiliensis*. Biochem J 124:407–417.
19. Byres E, Alphey MS, Smith TK, Hunter WN (2007) Crystal structures of *Trypanosoma brucei* and *Staphylococcus aureus* mevalonate diphosphate decarboxylase inform on the determinants of specificity and reactivity. J Mol Biol 371:540–553.
20. Vinokur JM, Korman TP, Cao Z, Bowie JU (2014) Evidence of a novel mevalonate pathway in archaea. Biochemistry 53:4161–4168.
21. Dhe-Paganon S, Magraph J, Abeles RH (1994) Mechanism of mevalonate pyrophosphate decarboxylase: evidence for a carbocationic transition state. Biochemistry 33:13355–13362.
22. Azami Y, Hattori A, Nishimura H, Kawaide H, Yoshimura T, Hemmi H (2014) (R)-mevalonate 3-phosphate is an intermediate of the mevalonate pathway in *Thermoplasma acidophilum*. J Biol Chem 289:15957–15967.
23. Voynova NE, Fu Z, Battaile KP, Herdendorf TJ, Kim JP, Miziorko, HM (2008) Human mevalonate diphosphate decarboxylase: characterization, investigation of the mevalonate diphosphate binding site, and crystal structure. Arch Biochem Biophys 480:58–67.
24. Bonanno JB, Edo C, Eswar N, Pieper U, Romanowski MJ, Ilyin V, Gerchman SE, Kycia H, Studier FW, Sali A, Burley SK (2001) Structural genomics of enzymes involved in sterol/isoprenoid biosynthesis. Proc Natl Acad Sci USA 98:12896–12901.
25. Barta, ML, McWhorter WJ, Miziorko HM, Geisbrecht BV (2012) Structural basis for nucleotide binding and reaction catalysis in mevalonate diphosphate decarboxylase. Biochemistry 51:5611–5621.
26. Eisenberg D, Schwarz E, Komarony M, Wall R (1984) Amino acid scale: normalized consensus hydrophobicity scale. J Mol Biol 179:125–142.
27. Jorda J, Yeates TO (2011) Widespread disulfide bonding in proteins from thermophilic archaea. Archaea 2011:409156.
28. Beeby M, O'Connor BD, Ryttersgaard C, Boutz DR, Perry LJ, Yeates TO (2005)The genomics of disulfide

bonding and protein stabilization in thermophiles. PLoS Biol 3:e309.
29. Mallick P, Boutz DR, Eisenberg D, Yeates TO (2002) Genomic evidence that the intracellular proteins of archaeal microbes contain disulfide bonds. Proc Natl Acad Sci USA 99:9679–9684.
30. Cheek S, Zhang H, Grishin NV (2002) Sequence and structure classification of kinases. J Mol Biol 320:855–881.
31. Andreassi JL, Leyh TS (2004) Molecular functions of conserved aspects of the GHMP kinase family. Biochemistry 43:14594–14601.
32. Qiu Y, Gao J, Guo F, Qiao Y, Li D (2007) Mutation and inhibition studies of mevalonate 5-diphosphate decarboxylase. Bioorg Med Chem Lett 17:6164–6168.
33. Krepkiy D, Miziorko HM (2004) Identification of active site residues in mevalonate diphosphate decarboxylase: implications for a family of phosphotransferases. Protein Sci 13:1875–1881.
34. Zhou T, Daugherty M, Grishin NV, Osterman AL, Zhang H (2000) Structure and mechanism of homoserine kinase: prototype for the GHMP kinase superfamily. Structure 8:1247–1257.
35. Potter D, Miziorko HM (1997) Identification of catalytic residues in human mevalonate kinase. J Biol Chem 272:25449–25454.
36. Andreassi JL, Vetting MW, Bilder PW, Roderick SL, Leyh TS (2010) Structure of the ternary complex of phosphomevalonate kinase: the enzyme and its family. Biochemistry 48:6461–6468.
37. Vannice JC, Skaff DA, Keightley A, Addo J, Wyckoff GJ, Miziorko HM (2013) Identification in *Haloferax volcanii* of phosphomevalonate decarboxylase and isopentenyl phosphate kinase as catalysts of the terminal enzymatic reactions in an archaeal alternate mevalonate pathway. J Bacteriol 196:1055–1063.
38. Dellas N, Thomas ST, Manning G, Noel JP (2013) Discovery of a metabolic alternative to the classical mevalonate pathway. eLife 2:e00672.
39. Kelley LA, Sternberg MJE (2009) Protein structure prediction on the web: a case study using the Phyre server. Nat Protoc 4:363–371.
40. McPherson A (1982) Preparation and analysis of protein crystals. New York: Wiley.
41. Kabsch W (2010) XDS. Acta Crystallogr D Biol Crystallogr 66:125–132.
42. Keegan RM, Winn MD (2007) Automated search-model discovery and preparation for structure solution by molecular replacement. Acta Cryst D63:447–457.
43. McCoy AJ, Grosse-Kunstleve RW, Adams PD, Winn MD, Storoni LC, Read RJ (2007) Phaser crystallographic software. J Appl Crystallogr 1:658–674.
44. Stein, ND (2008) CHAINSAW: a program for mutating pdb files used as templates in molecular replacement. J Appl Cryst 41:641–643.
45. Murshudov GN, Vagin AA, Dodson EJ (1997) Refinement of macromolecular structures by the maximum-likelihood method. Acta Crystallogr D Biol Crystallogr 53:240–255.
46. Cowtan K (2006) Buccaneer software for automated model building. Acta Cryst D62:1002–1011.
47. Langer G, Cohen SX, Lamzin VS, Perrakis A (2008) Automated macromolecular model building for x-ray crystallography using ARP/wARP version 7. Nat Protoc 3:1171–1179.
48. Emsley P, Lohkamp B, Scott WG, Cowtan K (2010) Features and development of Coot. Acta Crystallogr D Biol Crystallogr 66:486–501.
49. Afonine PV, Grosse-Kunstleve RW, Echols N, Headd JJ, Moriarty NW, Mustyakimov M, Terwilliger TC, Urzhumtsev A, Zwart PH, Adams PD (2012) Towards automated crystallographic structure refinement with phenix.refine. Acta Cryst D68:352–367.
50. Laskowski RA, MacArthur MW, Moss DS, Thornton JM (1993) PROCHECK: a program to check the stereochemical quality of protein structures. J Appl Cryst 26: 283–291.
51. Colovos C, Yeates TO (1993) Verification of protein structures: patterns of nonbonded atomic interactions. Protein Sci 2:1511–1519.
52. Lüthy R, Bowie JU, Eisenberg D (1992) Assessment of protein models with three-dimensional profiles. Nature 356:83–85.
53. The PyMOL Molecular Graphics System, Version 1.4, Schrödinger, LLC. Available at: http://www.pymol.org.
54. Automated design of mutagenic primers for site-directed mutagenesis, PrimerX, 2014 Version, Carlo Lapid. Available at: http://www.bioinformatics.org/primerx/.
55. Pei J, Kim BH, Grishin VN (2008) PROMALS3D: a tool for multiple sequence and structure alignment. Nucl Acids Res 6:2295–2300.
56. Macromedia Fireworks MX 2004, Version 7.0, Adobe Systems Inc. Available at: http://www.adobe.com.
57. Gouet P, Robert X, Courcelle E (2003) ESPript/ENDscript: extracting and rendering sequence and 3D information from atomic structures of proteins. Nucl Acids Res 13:3320–3323.